

Aerodynamic modeling of the Yigong gigantic rock slide-debris avalanche, Tibet, China

Yueping Yin · Aiguo Xing

Received: 10 December 2009 / Accepted: 12 December 2010 / Published online: 8 February 2011
© Springer-Verlag 2011

Abstract On the April 9 of 2000, a gigantic rapid rock slide-debris avalanche occurred in Bomi, Tibet. Some $280\text{--}300 \times 10^6 \text{ m}^3$ of material travelled 10 km within 10 min and dammed the Yigong River, forming a $2.9 \times 10^9 \text{ m}^3$ barrier lake. Wind tunnel testing was undertaken to determine the aerodynamic parameters involved, from the initial rock slide-fall to its point of impact. The paper reports the numerical analyses undertaken and discusses the significance of the air-cushion effect. It is concluded that Yigong rapid rock slide-debris avalanche “flew” in the air for about 12.9 s from its detachment from the source to its collision with the floor of the Zamunong gully at 3,317 m asl. The velocity of the avalanche mass at the point of detachment was some 81.8 m/s and the collision velocity approximately 117 m/s.

Keywords Avalanche · Debris flow · Rapid long run-out · Air-cushion effect · Wind tunnel test · Aerodynamics

Résumé Le 9 avril 2000, une énorme et rapide avalanche rocheuse a eu lieu à Bomi, au Tibet. Environ 280 à 300 millions de m^3 ont parcouru 10 km en 10 mn et barré la rivière Yigong, formant un lac de barrage de 2,9 milliards de m^3 . Des essais en soufflerie ont été réalisés afin de déterminer les paramètres aérodynamiques impliqués,

depuis la zone de départ du glissement rocheux jusqu’à la zone d’arrivée des dépôts. L’article présente les analyses numériques réalisées et discute de l’importance de l’effet de coussin d’air. On conclut que le glissement rocheux—avalanche de roche de Yigong a « volé » dans l’air pendant environ 12,9 s depuis son départ de la zone source à son point d’impact avec le terrain de la gorge de Zamunong à la cote 3,317 m asl. La vitesse de la masse avalancheuse au point de départ de la zone source était d’environ 81,8 m/s et la vitesse au point d’impact approximativement 117 m/s.

Mots clés Avalanche rocheuse · Ecoulement de débris · Propagation rapide · Effet de coussin d’air · Essai en soufflerie · Aérodynamique

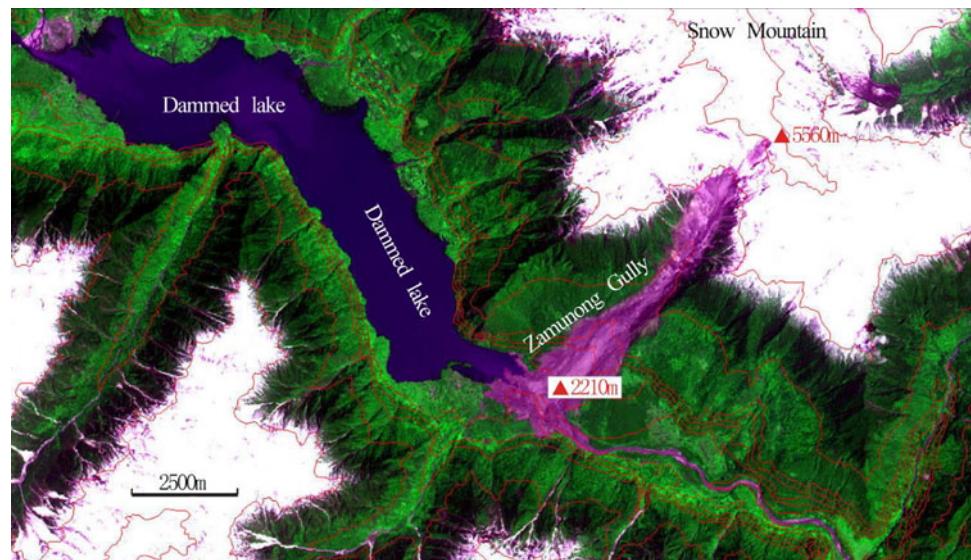
Introduction

Since the famous Vaiont catastrophic rockslide on 9 October 1963, the failure mechanism, the rapid long run-out effects and the surge movement of that avalanche have been the object of much study. Kent (1966) proposed that entrapped air could fluidise broken rock and Shreve (1968) suggested that a cushion of entrapped air would encourage avalanche movement. Lu (1991) analyzed the high-speed motion of a rock mass in the air in terms of plane wing theory, quantitatively examined the mechanism of “air born” movement and obtained a prediction formula for the sliding speed and distance during the long run-out movement. The sliding mass could be characterized as a turbulent avalanche-debris flow, which is very different from conventional landslides. For example, where the extremely rapid and long run-out avalanches or rockfalls triggered by the Wenchuan Earthquake occurred along the main seismic fault, the maximum sliding velocity was estimated to

Y. Yin (✉)
China Geological Survey, 45 Fuwai Dajie, Xicheng District,
Beijing 100037, China
e-mail: yyueping@mail.cgs.gov.cn

A. Xing
Shanghai Jiao Tong University, 800 Dongchuan Road,
Minhang District, Shanghai 200240, China
e-mail: xingaiquo@sjtu.edu.cn

Fig. 1 Remote sensing image shown the Yigong rock slide-debris avalanche and dammed lake



be >70 m/s as a consequence of the >1.5 g earthquake acceleration, while due to the lubrication effect of the air layer, the run-out distance (accumulation) was many times the difference in height from the upper fracture to the elevation of the ground below (Yin et al. 2009).

Huge avalanches can reach a high velocity during the sliding stage. If the difference between the height of the source area and the accumulation area is sufficiently great, the sliding mass can act in part as a flying object with a velocity similar to the gliding speed of an aircraft at take-off or landing (Xing et al. 2002). If the differential elevation is small, the airflow below the moving mass is confined by the sides of the valley, which increases the pressure at the base of the avalanche mass, hence its lifting force, providing air lubrication for the long run-out. In view of the initial earthquake motion, even at the beginning of the failure the movement is at high speed, throwing/ejecting material, characteristic of an air-cushion effect (Huang 2009).

The details of the air-cushion effect are still vague. Having analysed a large number of avalanches, including those which occurred on the moon where the air effect would not apply, Hsu (1975) preferred the mass flow of concentrated cohesionless grains to explain the sturzstrom flow, rather than air-lubrication. The coefficient friction angle (Scheidegger 1973) and the motion of a cohesionless granular avalanche (Davies et al. 1999) cannot explain the run-out of the Yigong rock slide-debris avalanche.

The present research used wind tunnel modeling and numerical analysis based on aerodynamic theory to study the air-cushion effect of rapid long run-out avalanches using the Yigong rock slide-debris avalanche as an example. It should be noted that as the air-cushion effect occurs with the first collision with the lateral sides and not during



Fig. 2 Yigong rock slide-debris avalanche

all four stages of the Yigong rock slide-debris avalanche, the aerodynamics theory was only applied to the process from the initial rock slide-fall stage along a wedge-shaped bedrock shear to the first collision with the valley sides.

General characteristics of the Yigong avalanche

On 9 April 2000, a gigantic rock slide-debris avalanche occurred at the Yigong River in Bomi County, Tibet. The avalanche took only 10 min to travel a horizontal distance of 10 km through a vertical elevation of 3,330 m (5,520 m asl at the source to 2,190 m asl at the lobe; Fig. 1). The avalanche dammed the Yigong River and created a large barrier lake. The 280–300 million m^3 avalanche deposit is about 2,500 m long and 2,500 m wide. With an average thickness of 60 m, it covers an area of about 5 km^2 (Fig. 2).

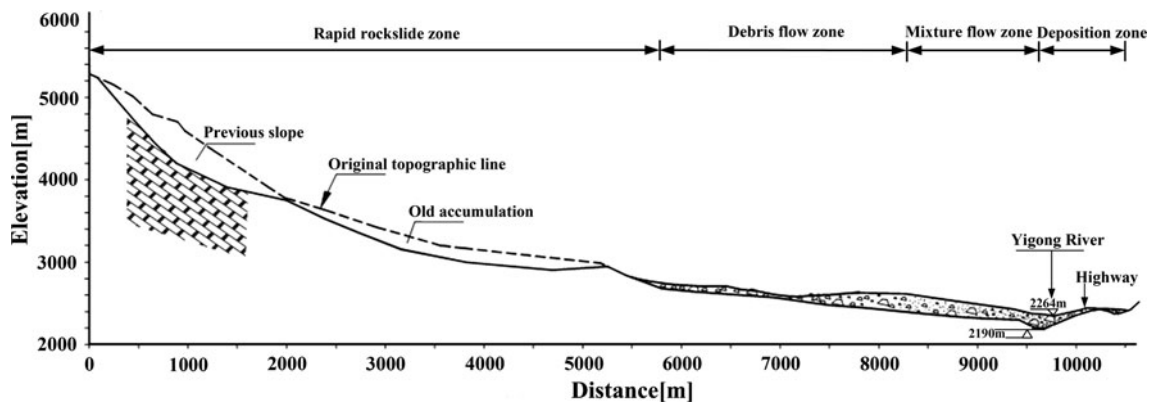


Fig. 3 Cross section of the Yigong rock slide-debris avalanche, Bomi County



Fig. 4 The upper part of trees truncated by the “flying” avalanche while lower part remains

As a result of the retreat of the snow line, a wedge-shaped, water-saturated rock mass of some 100 million m^3 slid out of the Zemunong gully, towards the Yigong River, from an elevation of approximately 5,520 m asl. Using the nomenclature of Yin et al. (2009), the rock slide-debris avalanche can be divided into four stages: the initial rockslide movement through the wedge-shaped bedrock; the debris flow with an air-cushion; the multi-phase mixture stream with broken rock, glacial soil, snow-melt water and the heat of evaporation; and the surge and scatter deposition (Figs. 3, 4).

1. The initial rockslide-fall

A wedge-shaped rock mass slid down along steeply inclined strata with a dip angle of about $70\text{--}80^\circ$ from a snow-covered mountain at an elevation of $>5,520$ m asl, with the sound of thunder and light flashes. The horizontal sliding distance of the layered marble, slate and granite was some 2,500 m. With the covering of ice and snow, the volume was some 200 million m^3 (Fig. 5).

2. The debris flow

The extremely rapid sliding mass collided forcefully with previous landslide and glaciofluvial deposits, carrying with it the earlier disturbed material and transporting it into the river with tremendous kinetic energy. The sliding mass continued to fly forward at high speed as a result of the air-cushion effect, rather than forming a traditional “sliding zone”. The mass of disintegrated granite, marble and slate slid forward for $>2,000$ m and came to rest at the entrance of the valley on the left bank.

3. The mixture flow zone

The impacted previous deposits (glaciofluvial and old landslide material) were thrown forward at high speed and collided with each other, such that they were heated or even melted and disintegrated. The strong air blast snapped off and defoliated many trees (Fig. 4) although the lower part and roots remained. This 30–40 m long accumulation zone is composed of mixed soil and rocks.

4. The deposition zone

The moving material collided at high speed with the old landslide material on the right bank, forming a mixture of mud, rock, water and air >200 m thick. A portion of the moving mass extended some 150 m onto the old disturbed material and destroyed much of the dense pine forest before it was converted into a debris flow with a volume of 5 million m^3 . This extended to the bridge near the Tea Factory of Yigong, about 200 m from houses. Some of the material flowed back and was deposited on the new avalanche accumulation where it was converted into a mud/rock flow moving both downstream and upstream.

The accumulation of large rocks and loose debris dammed the Yigong River. This landslide dam is extremely irregular in shape but has a width of 2,200–2,500 m at its base, a length of 1,000 m, a top width of 200 m and an area of 2.5 km^2 . Downslope, the distance in height between the

Fig. 5 Wedge-shaped sliding source area of the Yigong avalanche

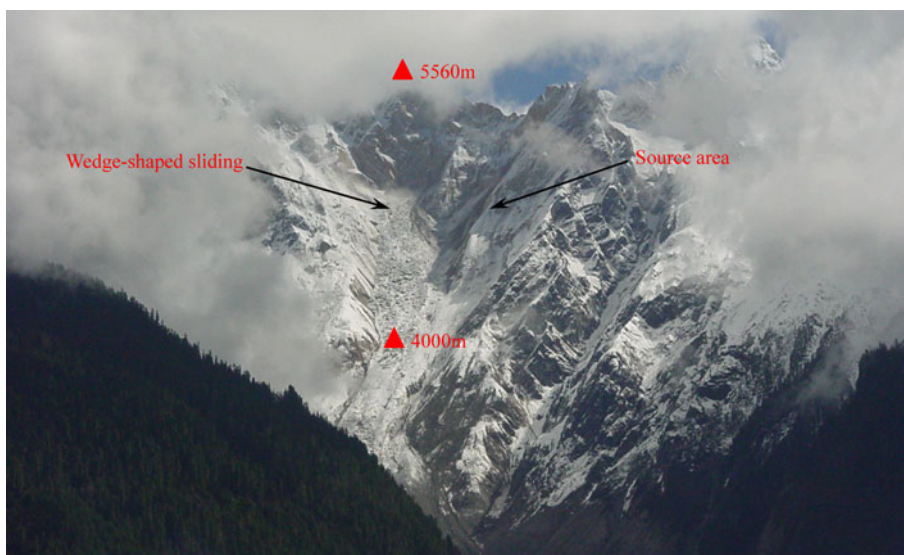
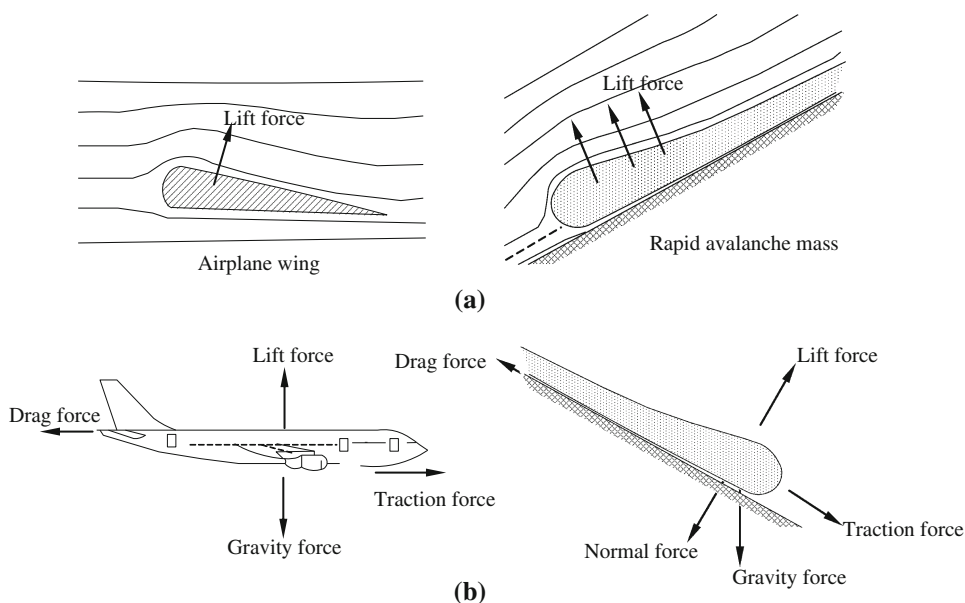


Fig. 6 Air-cushion effect
a Comparison of aerodynamic profiles for an airplane wing and a large avalanche;
b Comparison of force components for an airplane and a large avalanche



floor of the valley and the top of the dam was 90 m; the water level being some 35 m below the top of the saddle. The upstream and downstream slopes of the accumulation average 5° and 8° respectively.

Wind tunnel test

Basic concept model of the air-cushion effect on avalanche “flying”

Where “trap” topography (such as a canyon) occurs, air is entrained at the underside of the dislodged mass moving out from upslope, which leads to a complicated aerodynamic phenomenon. Regardless of its inner structure and

state, it could be conceptually regarded as an entity, “flying” in the air. Consequently, the avalanche mass is subjected to gravity, drag and lift forces due to the high-speed air-cushion effect between the lower surface of the avalanche mass and the valley.

The avalanche mass can therefore be considered as some kind of airfoil wing, i.e., the longitudinal length of avalanche is equivalent to the wing chord, and its length perpendicular to the vertical section is equivalent to the wing span (Fig. 6). It is therefore suggested that aerodynamic theory and wing modeling can be used to analyze the air-cushion effect. Wind tunnel modeling of a wing similar to the avalanche mass allows the aerodynamic parameters of the “flying” avalanche mass to be determined. Aerodynamic force, flying velocity and flying distance of the



Fig. 7 Avalanche model for free flow testing

high-speed long run-out avalanche can then be estimated by aerodynamic numerical analysis.

Equipment

The experiment was carried out in the second section of the single reflux duplex industrial wind tunnel (XNJD-1) at Southwest Jiaotong University, Chengdu. The test section is a rectangle, 2.4 m wide and 2 m high, with wind speeds of between 45 and 0.5 m/s. The wind tunnel has a support system, force balance system and simultaneous fluctuating pressure measurement system. The model had a gradient (α) between 12° and 20° . The designed loads of the three component box-type strain balances used to measure the aerodynamic force are: drag force (thrust) $X = 50$ kgf, lift force $Y = 120$ kgf and moment $M_z = 12$ kg·m. The measuring range of the pressure sensor is 1 kPa.

A 590×232 mm \times 120 mm, wooden model was designed based on the remote sensing image data of the Yigong rock slide-debris avalanche; the geometric scale ratio is 1:2500 (Fig. 7). The lift force corresponds to the lateral force of the model and the pitching moment corresponds to the torque around the supporting bar of the model.

Method

The testing program preset variable angles for the avalanche under a given air velocity. The angle of the avalanche movement was gradually changed until data had been obtained for all the pre-determined angles. Although the maximum wind speed of the wind tunnel was 45 m/s, it was considered that $1/3$ – $2/3$ of the maximum would be the ideal speed range for the testing, i.e., 15–30 m/s. Most Chinese researchers use a sliding speed of >10 – 20 m/s as the lower limit of a high-speed landslide (Yin et al. 2009).



Fig. 8 Avalanche mirror model for ground effect testing

The aerodynamic force of the wing model of the avalanche mass was measured at intervals of $\Delta\alpha = 2^\circ$.

As noted above, when the high-speed avalanche mass is 1–2 wing spans away from the valley, the topographic effect changes the airstream on the surface of the avalanche mass. A mirror image method was applied to test the topographic effect. The model to be measured and the mirror model were placed symmetrically at a certain distance away from each other (Fig. 8) and the aerodynamic forces of the avalanche mass measured as the distance and angle were changed. The testing wind speed was 30 m/s, the angle of the avalanche movement between 12 – 20° and the change interval, $\Delta\alpha = 4^\circ$. The wing span of the avalanche was 23 cm and the distance between the wing models 24, 33, 42, 51 and 60 cm. Due to the limitations of the testing conditions, only one model was rotating during the testing process.

Results and analysis

Figure 9 presents a characteristic aerodynamic curve of the wing model for the free flow test. As seen in Fig. 6, the lift coefficients of the landslide wing model increase with increasing angle of movement (correlation coefficient 0.997). The lift-drag ratio exhibits an approximately linear change. With the increase in angle of movement, the lift-drag ratio increases slowly. The moment coefficients of the landslide wing model all decrease with the increase of the model angle of attack. The moment coefficient and the angle of attack show a relationship of second-degree parabola, with the correlation coefficient of 0.999.

Figure 10a gives the variation curves of the lift coefficient with the angle of attack and the distance of the modeled landslide wing. It can be seen that the lift coefficient increases with increasing angle of attack. Compared to the free flow testing, there is a marked increase in the

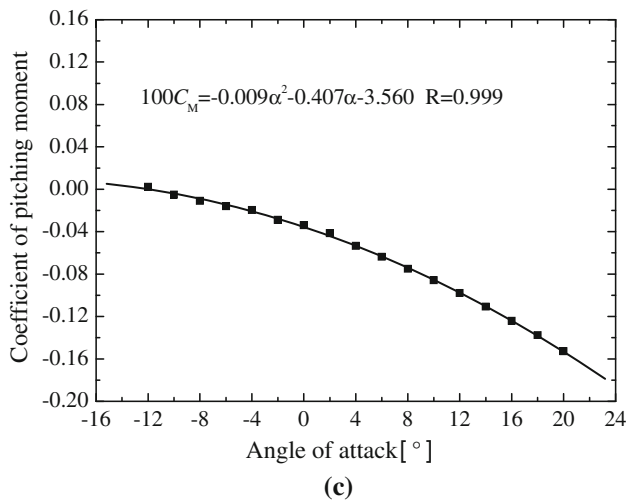
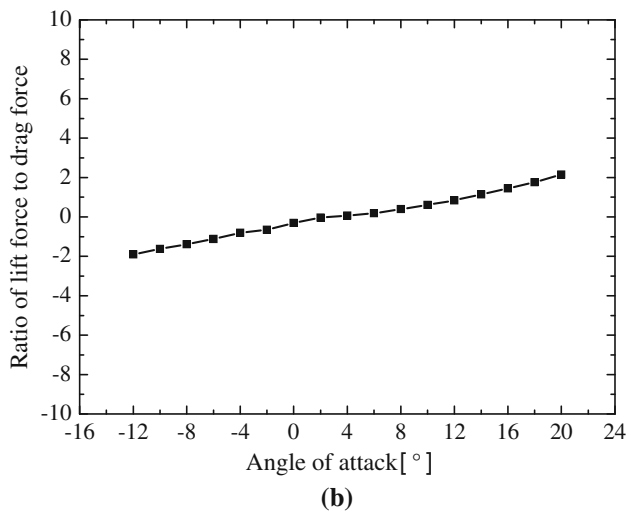
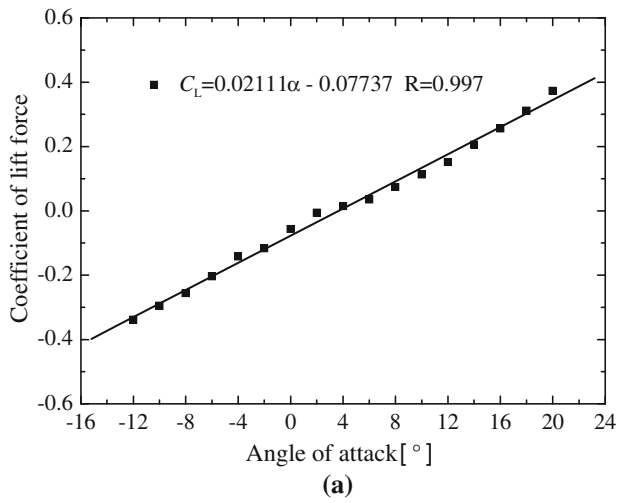


Fig. 9 Aerodynamic characteristic curve of avalanche wing model for the free flow testing. **a** Coefficient of lift force. **b** Ratio of lift force to drag force. **c** Coefficient of pitching moment

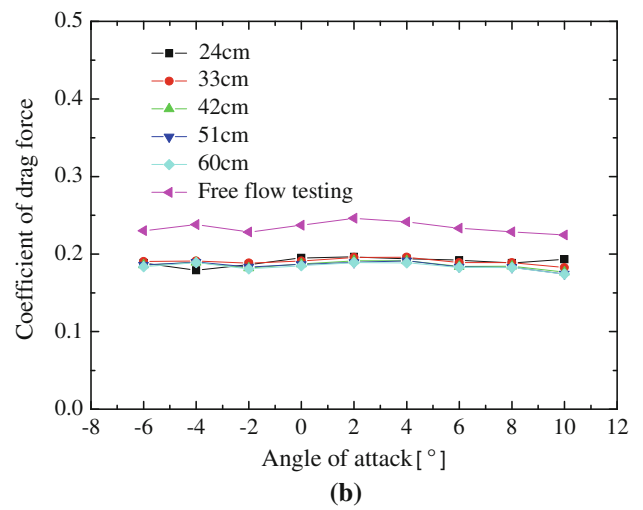
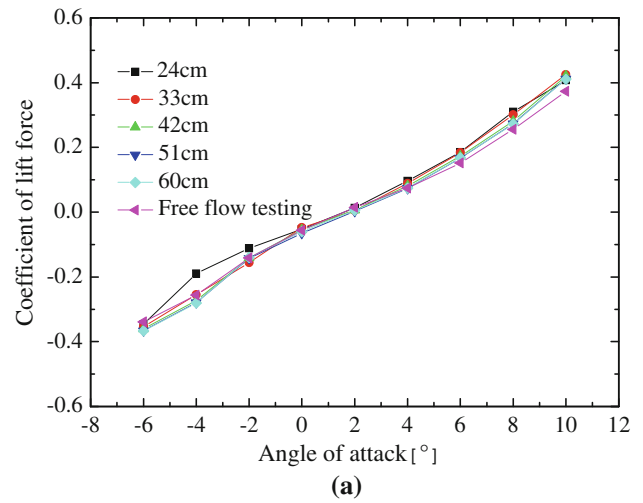


Fig. 10 Aerodynamic characteristic curve of avalanche wing model for the ground effect testing. **a** Coefficient of lift force. **b** Coefficient of drag force

slope of the lift curve under the ground effect. The lifting coefficient may have a positive or negative effect. The landslide wing model has an asymmetrical shape and the critical point of the positive and negative effects of the lift force is with an angle of attack of $c. 1^\circ$. After the critical point, as the angle of attack increases, the ground effect coefficient changes between 3.68–6.86 while with the decrease of the distance between the models, the lift coefficient exhibits an increasing trend.

Figure 10b gives the variation curves of the drag coefficient with the angle of attack and the distance between the models. With the ground effect, the drag coefficient decreases by about 25% compared to that in the free flow testing, but the effect of the distance between the models on the drag coefficient is insignificant.

Fig. 11 Sketch illustrating the avalanche mass “flying” without air-cushion effect

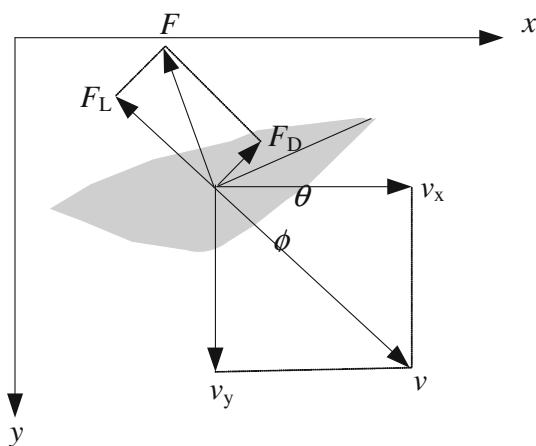
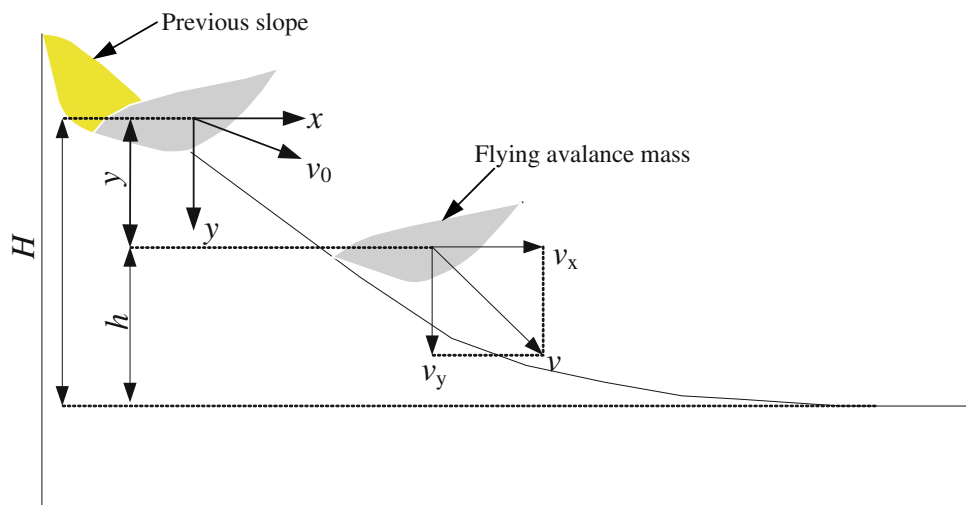


Fig. 12 Sketch showing force of the rapid avalanche mass “flying”
 a Without air-cushion effect b With air-cushion effect

Numerical analysis of the Yigong avalanche movement

Establishing an equation for the avalanche flying

The Yigong rock slide-debris avalanche appeared to “fly” after falling from the source area at high speed. The aerodynamic forces involved are similar to those at the take-off or landing of aircraft. While “flying” at high speed, the avalanche mass did not disintegrate but remained relatively intact, hence it can be regarded as a rigid body when considering the flying state equation of its center of mass. The source area of the rock slide-debris avalanche is taken as the origin point “O” to build the coordinate system during the avalanche “flying”, with the horizontal direction on the *x*-axis and vertical direction on the *y*-axis (Fig. 11).

Flying equation without air-cushion effect

When the high-speed rock slide-debris avalanche detached from the source, it could be assumed that the initial velocity of the center of the avalanche mass is v_0 , the angle between v_0 and the horizontal axis ox is φ_0 (Fig. 11). Without the air-cushion effect, the motion of the center of mass during the avalanche flying could be regarded as projectile motion under the effect of gravity, thus, the motion equation of the center of the avalanche mass was expressed as:

$$\left. \begin{aligned} v_x &= v_{0x} = v_0 \cos \varphi_0 \\ v_y &= v_{0y} + gt = v_1 \sin \varphi_0 + gt \\ x &= v_0 \cos \varphi_0 \cdot t \\ y &= v_1 \sin \varphi_0 \cdot t + \frac{1}{2}gt^2 \end{aligned} \right\}$$

where v_x and v_y are the horizontal flight velocity and vertical flight speed of the avalanche mass center in the air respectively, g is acceleration of gravity, t is the flying time and x, y denote the spatial coordinates of the avalanche.

Flying equation with air-cushion effect

Figure 12 is a sketch map indicating the forces involved in the high-speed avalanche mass flying.

The results of the above wind tunnel testing indicate that the lift coefficient of the avalanche mass increases under the ground effect, whereas the drag change is not significant. As consequence, the ground effect coefficient G_e is added to the calculation formula for the lift force on the basis of the result of the free flow testing. The calculating formulae of the parameters are as follows,

$$\left. \begin{aligned} F_L &= \frac{1}{2} G_e C_L(\alpha) \rho S v^2 \\ F_D &= \frac{1}{2} C_D(\alpha) \rho S v^2 \\ M_Z &= \frac{1}{2} C_M(\alpha) \rho S v^2 \\ \tan \phi &= \frac{dy}{dx} \\ v^2 &= \left(\frac{dx}{dt}\right)^2 + \left(\frac{dy}{dt}\right)^2 \\ \alpha &= \theta - \phi \end{aligned} \right\}$$

where x, y are spatial coordinates and v is the resultant velocity of the center of avalanche mass, F_L, F_D, M_Z are the lift force, drag force and pitching moment, C_L, C_D, C_M are coefficients of the lift force, drag force and pitching moment of the avalanche mass, G_e, ρ are the ground effect coefficient and air density respectively, S is the avalanche mass projection area, θ is the angle between the avalanche mass axis and the horizontal direction, ϕ is the angle between the avalanche mass velocity direction v and the horizontal direction ($\tan \phi = \frac{dy}{dx}$), and α is the attack angle while the avalanche is flying.

As noted above, as the Yigong rock slide-debris avalanche remained relatively intact during flying, it could be regarded as a rigid body. The motion of a rigid body can be described by the motion equation of the base point and the rotation equation around the base point. For convenience, the center of mass is taken as the base point, hence the plane motion equation during the avalanche flying can be established as:

$$\left. \begin{aligned} F_L \sin \phi - F_D \cos \phi &= m \frac{d^2x}{dt^2} \\ mg - F_L \cos \phi - F_D \sin \phi &= m \frac{d^2y}{dt^2} \\ M_Z &= J_Z \frac{d^2\theta}{dt^2} \end{aligned} \right\}$$

where m, J_Z denote the mass and the inertia moment of the avalanche, respectively, and the relative parameters are as given above.

Numerical discretization of the avalanche flying equation

The plane motion equation of the avalanche flying is a system of implicit multivariate high-order partial differential equations. In view of the difficulty of undertaking the analytic solutions, numerical analysis was adopted to discretize the equation in the infinitesimal time interval (Δt) using a computer. In order to gain higher calculation accuracy, the four-order Runge–Kutta method is adopted; its discrete process is as follows:

$$\left. \begin{aligned} x' &= a \\ y' &= b \\ \theta' &= c \\ a' &= \frac{1}{m} (F_L \sin \phi - F_D \cos \phi) \\ b' &= g - \frac{1}{m} (F_L \cos \phi + F_D \sin \phi) \\ c' &= \frac{M_Z}{J_Z} \\ \tan \phi &= \frac{b}{a} \end{aligned} \right\} \Rightarrow \left. \begin{aligned} x_{n+1} &= x_n + \frac{\Delta t}{6} (k_{11} + 2k_{12} + 2k_{13} + k_{14}) \\ y_{n+1} &= y_n + \frac{\Delta t}{6} (k_{21} + 2k_{22} + 2k_{23} + k_{24}) \\ \theta_{n+1} &= \theta_n + \frac{\Delta t}{6} (k_{31} + 2k_{32} + 2k_{33} + k_{34}) \\ a_{n+1} &= a_n + \frac{\Delta t}{6} (k_{41} + 2k_{42} + 2k_{43} + k_{44}) \\ b_{n+1} &= b_n + \frac{\Delta t}{6} (k_{51} + 2k_{52} + 2k_{53} + k_{54}) \\ c_{n+1} &= c_n + \frac{\Delta t}{6} (k_{61} + 2k_{62} + 2k_{63} + k_{64}) \end{aligned} \right\} \Rightarrow$$

$$\left. \begin{aligned} k_{11} &= a_n & k_{21} &= b_n, & k_{31} &= c_n \\ k_{12} &= a_n + \frac{\Delta t}{2} k_{41} & k_{22} &= b_n + \frac{\Delta t}{2} k_{51} & k_{32} &= c_n + \frac{\Delta t}{2} k_{61} \\ k_{13} &= a_n + \frac{\Delta t}{2} k_{42} & k_{23} &= b_n + \frac{\Delta t}{2} k_{52} & k_{33} &= c_n + \frac{\Delta t}{2} k_{62} \\ k_{14} &= a_n + \Delta t k_{43} & k_{24} &= b_n + \Delta t k_{53} & k_{34} &= c_n + \Delta t k_{63} \end{aligned} \right\}$$

$$\left. \begin{aligned} k_{41} &= \frac{1}{m} \left(F_L \sin \left(\arctan \left(\frac{k_{21}}{k_{11}} \right) \right) - F_D \cos \left(\arctan \left(\frac{k_{21}}{k_{11}} \right) \right) \right) \\ k_{42} &= \frac{1}{m} \left(F_L \sin \left(\arctan \left(\frac{k_{22}}{k_{12}} \right) \right) - F_D \cos \left(\arctan \left(\frac{k_{22}}{k_{12}} \right) \right) \right) \\ k_{43} &= \frac{1}{m} \left(F_L \sin \left(\arctan \left(\frac{k_{23}}{k_{13}} \right) \right) - F_D \cos \left(\arctan \left(\frac{k_{23}}{k_{13}} \right) \right) \right) \\ k_{44} &= \frac{1}{m} \left(F_L \sin \left(\arctan \left(\frac{k_{24}}{k_{14}} \right) \right) - F_D \cos \left(\arctan \left(\frac{k_{24}}{k_{14}} \right) \right) \right) \end{aligned} \right\}$$

$$\left. \begin{aligned} k_{51} &= g - \frac{1}{m} \left(F_L \cos \left(\arctan \left(\frac{k_{21}}{k_{11}} \right) \right) + F_D \sin \left(\arctan \left(\frac{k_{21}}{k_{11}} \right) \right) \right) \\ k_{52} &= g - \frac{1}{m} \left(F_L \cos \left(\arctan \left(\frac{k_{22}}{k_{12}} \right) \right) + F_D \sin \left(\arctan \left(\frac{k_{22}}{k_{12}} \right) \right) \right) \\ k_{53} &= g - \frac{1}{m} \left(F_L \cos \left(\arctan \left(\frac{k_{23}}{k_{13}} \right) \right) + F_D \sin \left(\arctan \left(\frac{k_{23}}{k_{13}} \right) \right) \right) \\ k_{54} &= g - \frac{1}{m} \left(F_L \cos \left(\arctan \left(\frac{k_{24}}{k_{14}} \right) \right) + F_D \sin \left(\arctan \left(\frac{k_{24}}{k_{14}} \right) \right) \right) \end{aligned} \right\}$$

$$\left. \begin{aligned} k_{61} &= \frac{M_Z}{J_Z} \\ k_{62} &= \frac{M_Z}{J_Z} \\ k_{63} &= \frac{M_Z}{J_Z} \\ k_{64} &= \frac{M_Z}{J_Z} \end{aligned} \right\}$$

where Δt is the infinitesimal time interval, and a, b, c, k_{ij} ($i = 1, 2, 3, 4, 5, 6; j = 1, 2, 3, 4$) are intermediate variables during the discrete process, respectively.

In general, no matter whether the air-cushion effect is taken into consideration or not, the vertical displacement of the avalanche “flying” is a fixed value (measured value), and the other parameters are variable. The method of vertical displacement control was therefore adopted in this study, i.e. whether to exit the program was determined based on the vertical displacement of the avalanche in the air. When the vertical displacement is greater than or equal to the maximum height from the avalanche source area to the valley floor, the calculation will be stopped.

Selection of simulation parameters of the Yigong avalanche flying

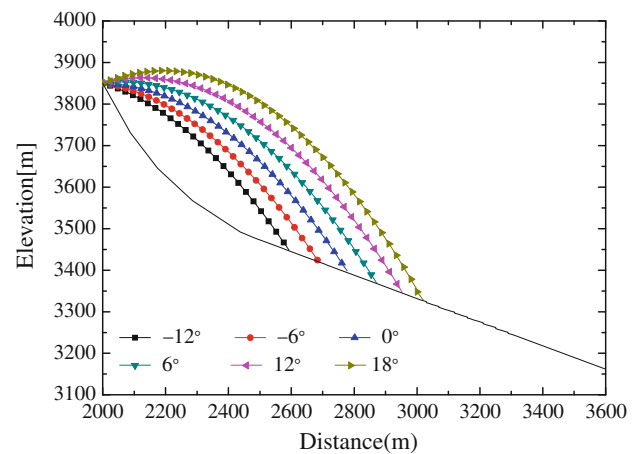
The rapid flying motion of the Yigong rock slide-debris avalanche was considered from the source area to its collision with the floor of the Zamunong gully. The aerodynamic characteristics are revised during the avalanche flying based on the free flow results from the wind tunnel testing and the irregular ground effect testing. The ground effect coefficient G_e takes the mean value 3.88, the modified lift coefficient $C_L = 0.081 \alpha - 0.299$, the drag coefficient changes slightly with the angle of attack, taking the mean value 0.182, and the moment coefficient $C_M = (-0.009\alpha^2 - 0.407\alpha - 3.560)/100$.

The initial rotation angle is $\theta_0 = 0^\circ$ and the time step $\Delta t = 0.1$ s. The avalanche velocity when leaving the source area is $v_0 = 81.83$ m/s, the volume is $c. 9.118 \times 10^7$ m³, the mass is 2.55×10^{11} kg, the moment of inertia is 3.15×10^{16} kg·m², the projection area is 0.691×10^6 m², and the air density 1.226 kg/m³ (Xing et al. 2002).

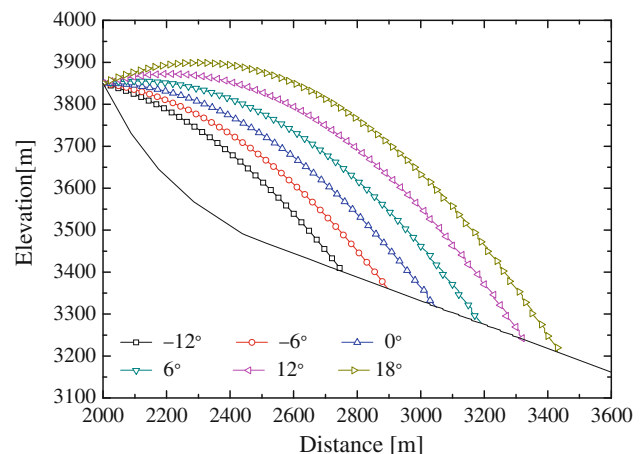
The wind tunnel testing indicated that the attack angle had a great effect on the aerodynamic characteristics of the avalanche, and different attack angles could lead to different motion trajectories and states. When the Yigong rock slide-debris avalanche moved from the source area, the initial attack angle was unknown hence different attack angles ($-12^\circ, -6^\circ, 0^\circ, 6^\circ, 12^\circ, 18^\circ$) were assumed in the calculations. The results were checked against the seismogram records triggered by the Yigong rock slide-debris avalanche in order to determine the most appropriate angle.

Numerical calculation results and analysis of the Yigong avalanche flying

The motion law of the center of the avalanche mass only is considered in this paper, without taking into account the motion of the various parts of the avalanche mass as it remained as an almost rigid body. Such parameters as displacement, velocity and acceleration were adopted to



(a) Without air-cushion effect



(b) with air-cushion effect

Fig. 13 Displacement curve for various angles of attack

reflect the high-speed avalanche flying situation in the air, and the results are compared with those obtained when ignoring the aerodynamic effect.

Displacement analysis

The displacement analysis results for the avalanche flying are shown in Figs. 13 and 14, which indicate that with the high speed air-cushion effect, the avalanche displacement is larger. The aerodynamic effect has a far greater influence on the horizontal displacement than on the vertical displacement while the increase in the failure angle at the source area significantly increases the aerodynamic effect. The initial failure angle has a remarkable effect on the trajectory and speed of the initial fall; the air-cushion effect is greater with increasing angle of attack such that there is a longer flying time and a further run-out distance.

During the whole Yigong rock slide-debris avalanche process, three significant ground motions were recorded in the seismic station at Nyingchi, Tibet. The time interval

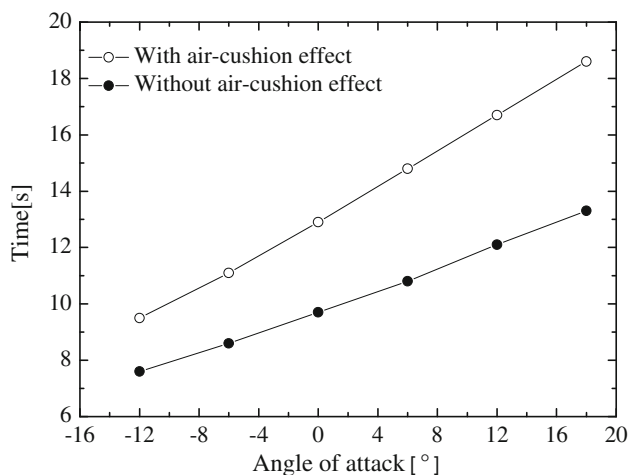


Fig. 14 “Flying” time for various angles of attack

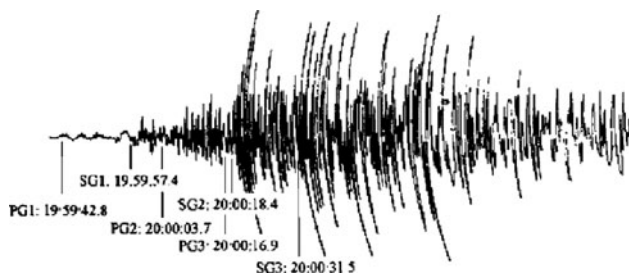


Fig. 15 Seismogram of the Yigong rock slide-debris avalanche recorded by the Linzhi seismic station (after Ren et al. 2001)

between the first and second peak motion was 29.9 s, and that between the second and third was 13.2 s (Fig. 15). The energy for the first motion was low, equivalent to a 2.9 magnitude earthquake. It is inferred that this motion was caused by a wedge-shaped mass sliding down two sets of fracture planes. The energies for the second and third motions were higher, equivalent to a magnitude 3.5 earthquake (Ren et al. 2001). It is likely the motions resulted from the impact of the avalanche mass and the lateral sides of the valley (second motion) and the floor of the valley (third motion), This is consistent with the collision simulated by numerical analysis which indicated 12.9 s when the initial angle of failure is vertical. As a consequence, to achieve the collision point in the valley of 3,317 m asl, it was necessary modify the flying direction in the analysis.

Velocity analysis

The time/velocity curves relative to elevation (Fig. 16) indicate little variation with different initial failure angles, with or without the air-cushion effect. Accordingly, only the velocity curve with a vertical initial failure angle is discussed in this paper. It can be seen from Fig. 16 that

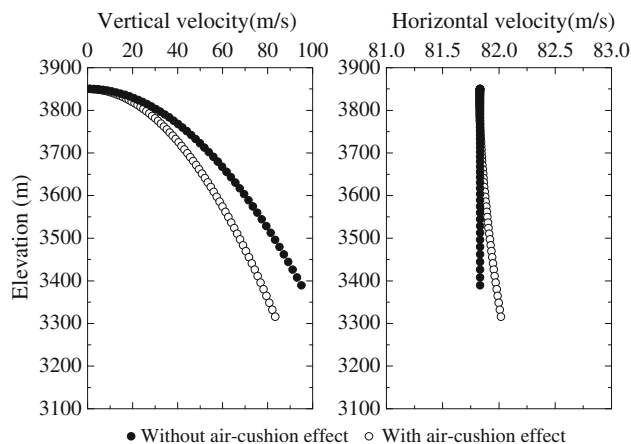


Fig. 16 Variation of velocity with elevation during the “flying” motion

both the vertical and horizontal velocity of the avalanche increases slightly under the effect of aerodynamic forces; with the decline in elevation, the difference in vertical velocity is larger. The implication of this is that the air lift forces help keep the material in the air, such that there is a longer flying time and further flying distance.

Based on the displacement analysis results, it is concluded that the Yigong rock slide-debris avalanche fell almost vertically from the source area, with a velocity at the center of the avalanche mass of about 117 m/s at the time it collided with the floor of the Zamunong gully.

Force-acceleration analysis

Generally speaking, the motion state of the object is determined by the force and the initial state. Therefore, in most cases, only the force or acceleration needs to be analyzed. But for the Yigong rock slide-debris avalanche, the acceleration and the force are not in the same direction in the coordinate system. The acceleration arises from components of gravity, lift force and drag force hence both the force and the acceleration need to be considered when analysing the motion of the avalanche mass. The calculated results are given in Figs. 17 and 18.

Figure 17 shows that, with the increase in velocity during the high-speed avalanche flying, the interaction between the avalanche and the air around it (especially the air-cushion underneath) becomes stronger. The influence of the lift is initially higher than that of the drag, to an elevation of approximately 3,700 m asl, below which the ratio changes such that the drag is more significant than the lift force; the lift-drag ratio reaching 20:1 when the rock slide-debris avalanche collided with the valley floor.

Figure 18 shows the aerodynamic effect on the acceleration of the rock slide-debris avalanche during its time in the air. The lift and drag induced by the air is small

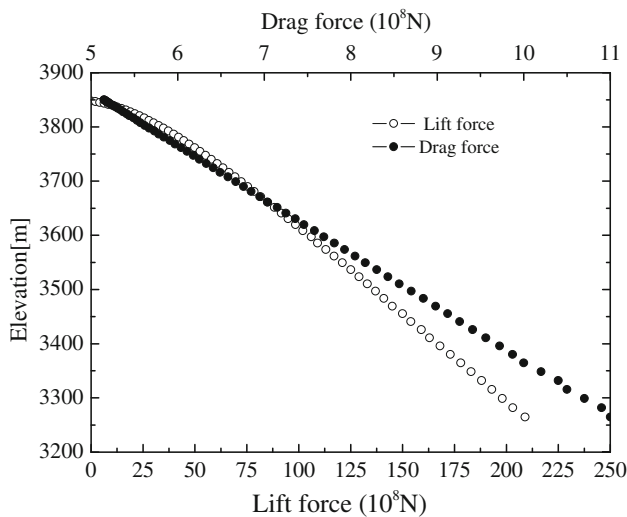


Fig. 17 Variation of aerodynamic force with elevation during the “flying” motion

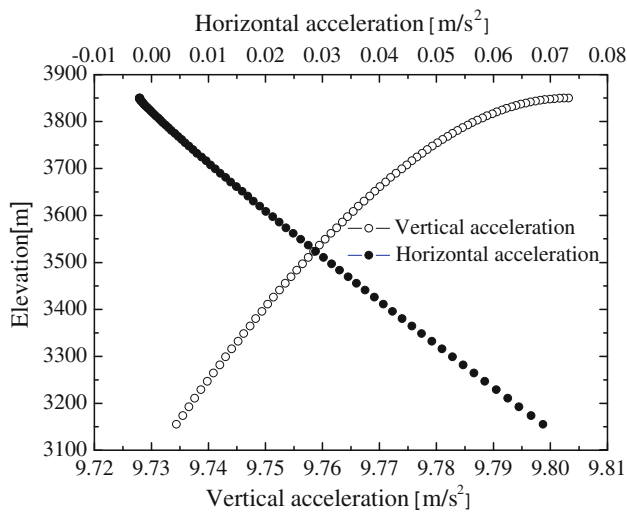


Fig. 18 Variation of acceleration with elevation during the “flying” motion

compared with the effect of gravity, with the maximum lift merely being 1% of the gravity. Therefore, initially the horizontal acceleration of the avalanche is close to 0 and gradually increases, whereas the vertical acceleration is approximate to the gravity acceleration, but gradually decreases.

Rotation angle analysis

During the high-speed flying, because the air-cushion effect has a pitching moment, the avalanche will have a certain degree of rotation (Fig. 19). Regardless of the initial angle of detachment from the source area, during the

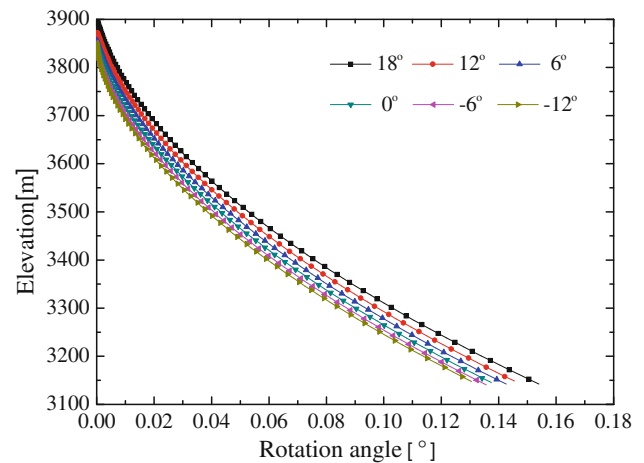


Fig. 19 Variation of rotation angle with elevation for different angles of attack

“flying” the rotation angle of the avalanche is very small. The computations indicated that for all six detachment angles analysed, the rotation angle did not exceed 0.2°. It must be appreciated that the actual avalanche is not a completely ideal rigid body, hence while the existence of the pitching moment may result in a certain degree of change in the distribution of the avalanche material, it does not make it rotate. As a consequence, the effect of the pitching moment in rotating the avalanche during its time in the air was not considered.

Energy analysis

During the flying motion, the potential energy can be converted into kinetic energy, gradually increasing the velocity of the avalanche. Because of the aerodynamic effect, there must be a certain degree of dissipation of the mechanical energy. The mechanical energy during the run-out at the rockslide stage is expressed as

$$E = E_g + E_k = mgh + \frac{1}{2}mv^2$$

The potential energy at 700 m down vertically from the detachment area was taken as zero while as there is little variation in mechanical energy with different angles of detachment, only a vertical initial angle of fall was considered. As seen in Fig. 20, the loss of mechanical energy during high-speed flying motion shows a linear trend, decreasing by some 23% during the whole process. The avalanche motion does not comply with the law of conservation of mechanical energy. The aerodynamic effect not only changes the motion path of the avalanche and increases the duration of the run-out, it also dissipates the mechanical energy of the avalanche mass.

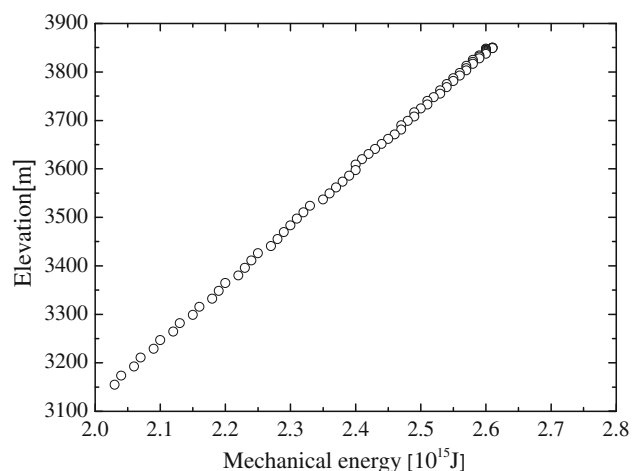


Fig. 20 Variation of mechanical energy with elevation during the “flying” motion

Conclusions

The Yigong rock slide-debris avalanche has been divided in four stages: the initial rockslide-fall along the wedge-shaped bedrock; an air-cushioned debris flow; the multi-phase mixture stream with broken rock, glacial soil, snow-melt water and heating evaporation; and the surge and scatter. The unexpectedly long run-out and fantastic speed of the Yigong rock slide-debris avalanche is difficult to elucidate using current theories regarding rapid long run-out avalanches, hence in this study wind tunnel modeling and numerical analysis were undertaken based on aerodynamic theory.

The results indicated that an avalanche mass with an air-cushion effect has a longer time and greater travel distance in the air compared to one where there is no air-cushion effect. It is concluded that the Yigong rapid rock slide-

debris avalanche was in the air for about 12.9 s from the time it detached from the source area until it collided with the floor of the Zamunong gully at some 3,317 m asl. The velocity of the rock slide-debris avalanche mass at its separation from the source area was some 81.8 m/s while at the point of collision with the gully it was some 117 m/s. The movement involved a vertical drop of 530 m and a horizontal sliding distance of 1,050 m.

References

- Davies TR, McSaveney MJ, Hodgson KA (1999) A fragmentation-spreading model for long-runout rock avalanches. *Canada J Geotechnics* 36:1096–1110
- Hsu KJ (1975) Catastrophic debris flow (Sturzstrom) generated by rockfalls. *Am Soc Geol Bull* 86:129–140
- Huang RQ (2009) Mechanism and geomechanical modes of landslide hazards triggered by Wenchuan 8.0 earthquake. *Chinese J Rock Mech Eng* 28(6):1239–1249 (in Chinese with English abstract)
- Kent PE (1966) The transport mechanism in catastrophic rock falls. *J Geol* 74:79–83
- Lu WN (1991) Aerodynamic approach to sliding problems of high-speed landslide. *J Xi’an Coll Geol* 13(4):78–85 (in Chinese with English abstract)
- Ren JW, Shan XJ, Shen J (2001) Geological characteristics and kinematics of the rock fall-landslide in Yigong, Southeastern Tibet. *Geol Rev* 47(6):642–647 (in Chinese with English abstract)
- Scheidegger AE (1973) On the prediction of the reach and velocity of catastrophic landslides. *Rock Mech* 5:231–236
- Shreve RL (1968) Leakage and fluidisation in air-layer lubricated avalanches. *Geol Soc Am Bull* 79:653–658
- Xing AG, Gao GY, Wu SM (2002) Study on wind tunnel testing of aerodynamic properties of high speed landslide flying. *J Tongji Univ* 30(5):435–836 (in Chinese with English abstract)
- Yin YP, Wang FW, Sun P (2009) Landslide hazards triggered by the 2008 Wenchuan earthquake, Sichuan, China. *Landslides* 6:139–152